

# Resonance enhancement effects in Raman-enhancing pyramid-like V-shape groove microstructures

Matyas Mechler and Sergei V. Kukhlevsky

*Department of Experimental Physics, University of Pécs, Pécs, Hungary*

Adam Mechler and Don McNaughton

*School of Chemistry, Monash University Clayton, VIC 3800, Australia*

Microscopic pyramidal pits in a reflective surface, a geometry similar to a retroreflector, are frequently used to enhance signal strength. The enhancement effect is generally attributed to surface plasmons, however, the sub-wavelength to near-wavelength dimensions of the pyramidal 3D geometry suggest contributions from diffraction and near-field effects. Our theoretical analysis of the light intensity distribution in the similar (but simpler) 2D geometry assuming a perfect conductor screen, that is, in the absence of any plasmon effects, shows that interference patterns forming within the cavity cause a significant resonant increase in local intensity. Such effect can be important for many applications, especially for the widely used Raman spectroscopy. Resonant enhancement without plasmons of the emitted Raman signal due to enhanced local field amplitude is also possible, which implies that the geometry practically implements a Raman laser. Comparison of diffraction patterns obtained with near-field and far-field approaches reveals that the near-field component is responsible for the observed dramatic intensity enhancement, and thus the Raman enhancement as well.

PACS numbers: 42.25.Bs, 78.67.-n, 42.55.Ye, 42.65.Dr

## INTRODUCTION

Micro- and nano-structured surfaces are frequently used to implement Surface Enhanced Raman Scattering (SERS), where interaction of the analyte with the substrate, mostly coupling between surface plasmons of the substrate and Raman modes of molecules [1, 2], lead to the multiplication of the Raman signal intensity. Controlling the SERS enhancement, however, has proven problematic due to the random plasmon distribution.

Nanovoids such as spheric cavities or grooves are known to host well-defined plasmon modes that interact strongly with incident laser light [2, 3]. It was thus proposed that nanovoids might be used to achieve tunable Raman enhancement [4]. One of the geometries that performs particularly well consists of an array of  $1\text{ }\mu\text{m}$  deep pyramidal pits of  $\sim 90^\circ$  opening angle [5]. Remarkably, this mesoscale geometry has reflecting surfaces of a distance that scales between a few wavelengths and sub-wavelength and thus resembles an (unstable) optical resonator. This raises the possibility that in this particular case the enhanced signal is generated by energy coupling into the Raman active medium from a high energy standing wave, practically implementing a Raman laser.

While parallel mirror micro-resonators have been studied before [6], the tilted mirror geometry of the pyramidal pit requires a different formalism to account for diffraction and near-field effects. Importantly, this geometry might be seen as a special case of an aperture (with an infinitesimally small opening at the tip of the pyramid). Light propagation through sub-wavelength apertures of various geometries is intensively studied due to the spe-

cial properties of the optical near field, in particular, light localization and the accompanying intensity enhancement [7, 8, 9, 10]. While experimental evidence proves its existence [10], the origin of the intensity enhancement is ambiguous as some theories attribute it to the excitation of surface plasmon polaritons [10, 11, 12, 13], others to intracavity (waveguide) resonances [14, 15, 16] or other phenomena [17, 18, 19]. While in the case of entirely sub-wavelength structures the comparable spatial distribution of plasmon- and diffraction-originated intensities prohibits an easy distinction, the dimensions of the pyramidal pit permit an attempt at the separation of the plasmon and diffraction effects.

When assuming that the aperture is in a perfect conductor screen, in which the plasmon frequency is infinity, purely diffractive intensity distributions might be calculated. The formulation we used is based on the near field treatment by Neerhoff and Mur [7, 20]. We intend to find if resonant enhancement does exist in a pyramid-type geometry, therefore we approximate the pyramidal pit with a V-slit, thus reducing the dimension of the problem to a plane, a simplification that, at the moment, is necessary for the solution of the problem. Importantly, the V-slit geometry is known to support standing waves as it can act as a waveguide; this application was discussed in a number of studies. [21, 22, 23, 24, 25]

## THEORY

In this section we summarize briefly the formulation used. For further details on a similar model see [7, 8]. The configuration is shown in Fig. 1. The slit is parallel

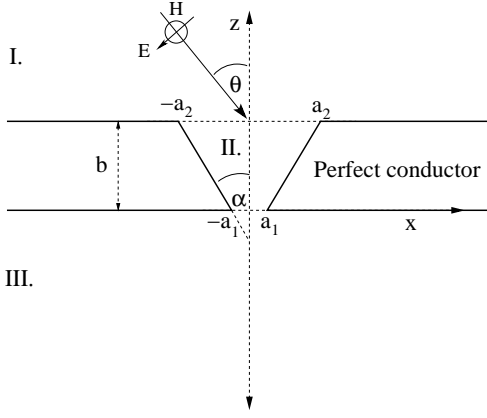


Figure 1: Aperture model of the pyramidal pit.

to the  $y$  axis in a screen of thickness  $b$ . The entrance width of the slit is  $a_2$ , the exit width is  $a_1$  (in our case,  $a_1 \rightarrow 0$ ). The geometry is divided into three regions: I)  $|x| < \infty$ ,  $|y| < \infty$ ,  $b < z < \infty$ , II)  $|x| < a_1 + \frac{a_2 - a_1}{b}z$ ,  $|y| < \infty$ ,  $0 < z < b$  and III)  $|x| < \infty$ ,  $|y| < \infty$ ,  $-\infty < z < 0$ .

An incident plane wave propagating in the  $x-z$  plane in region I arrives at the slit at an angle  $\theta$  with respect to the  $z$  axis. The time harmonic magnetic field is constant and at the same time polarized in the  $y$  direction:

$$\mathbf{H}(x, y, z, t) = U(x, z) \exp(-i\omega t) \vec{e}_y. \quad (1)$$

In this case the electric field can be found from Maxwell's equations, and the diffraction problem is reduced to one involving the single scalar field  $U(x, z)$  in Eq. (1) in only two dimensions. In the three regions the field is represented by  $U_j(x, z)$  ( $j = 1, 2, 3$ ). Due to time harmonicity the field satisfies the Helmholtz equation. In region I the field is composed of three components:  $U_1(x, z) = U^i(x, z) + U^r(x, z) + U^d(x, z)$ . Here  $U^i(x, z)$  is the incident field which is assumed to be a plane wave of unit amplitude:  $U^i(x, z) = \exp[ik_1(x \sin \theta - z \cos \theta)]$ .  $U^r(x, z)$  is the field that would be reflected without a screen:  $U^r(x, z) = U^i(x, 2b - z)$ . Finally,  $U^d(x, z)$  is the diffracted field produced by the presence of the slit.

For a perfectly conducting screen, the tangential  $\mathbf{E}$  vanishes at the surface ( $\partial_n U = 0$ ). Further boundary conditions result from assuming that the diffracted fields and their derivatives vanish at infinity. The final boundary condition is the continuity of the field and its derivative at the upper and lower slit boundaries. To find the field, the 2D Green's theorem is applied with one function given by  $U(x, z)$  and the other by a standard Green's function. We assumed that the tangential  $\mathbf{E}$  vanishes at the screen; therefore more is known about  $\partial_n U$  at the boundaries than is known about  $U$  itself. The Green functions for the V slit geometry can be found in [26].

The following boundary conditions are imposed on  $G$ :

$$\partial_z G_1(x, z)|_{z \rightarrow b+} = 0 \quad \text{for } |x| < \infty, \quad (2a)$$

$$\partial_z G_3(x, z)|_{z \rightarrow 0-} = 0 \quad \text{for } |x| < \infty, \quad (2b)$$

$$\partial_x G_2(x, z)|_{x \rightarrow (a_1 + \frac{a_2 - a_1}{b}z)^-} = 0 \quad \text{for } 0 < z < b, \quad (2c)$$

$$\partial_x G_2(x, z)|_{x \rightarrow (-a_1 - \frac{a_2 - a_1}{b}z)^+} = 0 \quad \text{for } 0 < z < b. \quad (2d)$$

$G_1$  and  $G_3$  must also satisfy the Sommerfeld radiation condition. Using these assumptions and conditions we may evaluate the three Green's functions. In regions I and III we find

$$G_1(x, z; x', z') = \frac{i}{4} [H_0^{(1)}(k_1 R) + H_0^{(1)}(k_1 R')], \quad (3a)$$

$$G_3(x, z; x', z') = \frac{i}{4} [H_0^{(1)}(k_3 R) + H_0^{(1)}(k_3 R'')], \quad (3b)$$

where

$$R = \sqrt{(x - x')^2 + (z - z')^2}, \quad (4a)$$

$$R' = \sqrt{(x - x')^2 + (z + z' - 2b)^2}, \quad (4b)$$

$$R'' = \sqrt{(x - x')^2 + (z + z')^2}. \quad (4c)$$

In region II, the method of images can be used:

$$G_2 = \pi i \sum_{n=-\infty}^{\infty} \left\{ H_0^{(1)}[k|\vec{r} - \vec{r}_n'] + H_0^{(1)}[k|\vec{r} - \vec{r}_n''] \right\}, \quad (5)$$

where  $\vec{r}_n'$  and  $\vec{r}_n''$  define a series of images reflected by the walls. The projection of an arbitrary point  $(x', z')$  on the wall:

$$x_{\times} = \frac{z' + x' \tan \alpha + \frac{a_1}{\tan \alpha}}{\frac{1}{\tan \alpha} + \tan \alpha}, \quad (6a)$$

$$z_{\times} = \frac{1}{\tan \alpha} \cdot (x_{\times} - a_1). \quad (6b)$$

From this the coordinates of the mirrored point are  $x_M = 2x_{\times} - x'$  and  $z_M = 2z_{\times} - z'$ . A series of images of the original point might be generated with the rotation of the points by  $4n\alpha$  ( $n$  being the number of rotation).

By using the definitions of the Green functions in the three regimes and the boundary conditions, one can find

the functions  $U^d$ ,  $U_2$ , and  $U_3$ :

$$U^d(x, z) = - \int_{-a_2}^{a_2} \frac{\epsilon_1}{\epsilon_2} G_1(x, z; x', b) DU_b(x') dx' \quad (7a)$$

for  $b < z < \infty$ ,

$$U_3(x, z) = \int_{-a_1}^{a_1} \frac{\epsilon_3}{\epsilon_2} G_3(x, z; x', 0) DU_0(x') dx' \quad (7b)$$

for  $-\infty < z < 0$ ,

$$U_2(x, z) = - \int_{-a_1}^{a_1} [G_2(x, z; x', 0) DU_0(x') - U_0(x') \partial_{z'} G_2(x, z; x', z')|_{z' \rightarrow 0+}] dx' + \int_{-a_2}^{a_2} [G_2(x, z; x', b) DU_b(x') - U_b(x') \partial_{z'} G_2(x, z; x', z')|_{z' \rightarrow b-}] dx' \quad (7c)$$

$|x| < a_1 + \frac{a_2 - a_1}{b} z$  and  $-\infty < z < 0$ ,

where the boundary fields are the same as in [7]:

$$U_0(x) = U_2(x, z)|_{z \rightarrow 0+}, \quad (8a)$$

$$DU_0(x) = \partial_z U_2(x, z)|_{z \rightarrow 0+}, \quad (8b)$$

$$U_b(x) = U_2(x, z)|_{z \rightarrow b-}, \quad (8c)$$

$$DU_b(x) = \partial_z U_2(x, z)|_{z \rightarrow b-}. \quad (8d)$$

By applying the continuity equations to these functions, a set of four integral equations can be found. We solved the equations for  $U^d$ ,  $U_2$ , and  $U_3$  numerically.

## RESULTS AND DISCUSSION

We analysed the light diffraction in region II for several laser wavelength in the range that is frequently used for Raman spectroscopy. A typical result is shown on Figure 2 for  $\lambda = 534$  nm. Similar resonant intensity enhancement was observed for all wavelengths. This enhancement is due to redistribution of electric charges (i.e. not plasmons) on the screen surface leading to standing wave formation with enhanced amplitude. The presence of the standing waves confirms that the geometry acts as an optical resonator.

Another interesting feature is the formation of vortices in the cavity (Figure 3). These vortices appear approximately at  $z \approx n\lambda/2$ , where  $n = 1, 2, 3, \dots$ . It is important to note that at the surface the electric field vectors are mostly parallel to the walls. Thus, when considering the interaction with the Raman active material, the enhancement of different modes should occur in comparison to plasmon-enhancement where the electric field is mostly perpendicular to the surface.

Far-field theory also predicts the standing waves and the vortices (Fig. 4), however, a few remarkable differences justify the use of near-field theory. First, at the

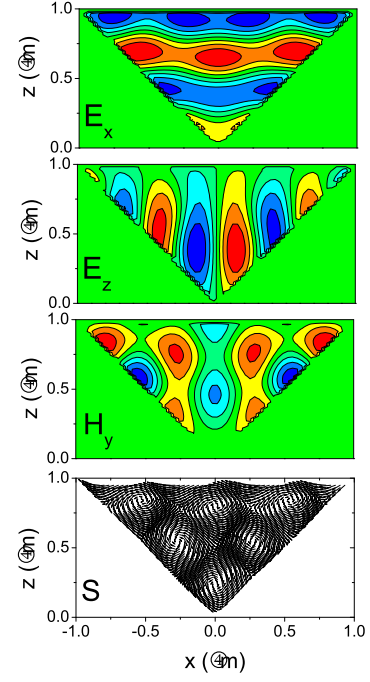


Figure 2:  $E_x$  and  $E_z$  electric and  $H_y$  magnetic field distributions, and the electric field vector in the V-groove for  $\lambda = 534$  nm.

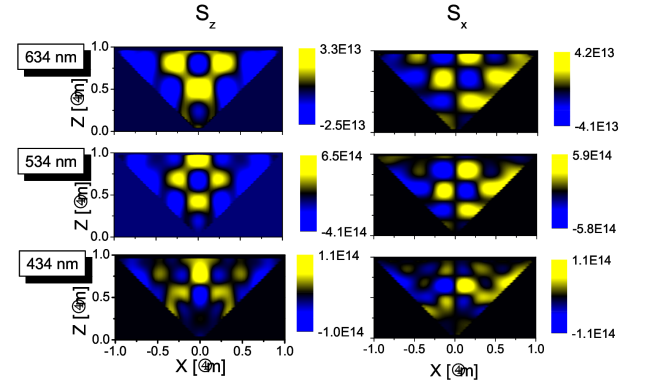


Figure 3: Electric field vectors for three wavelengths: 434 nm, 534 nm and 634 nm.

slit entrance ( $z \rightarrow b^-$ ) a strong intensity suppression can be observed (see Figs. 5 and 3) that cannot be seen in the case of a macroscopic slit with the same geometry (see Fig. 4). Notably, far-field diffraction theory used to calculate intensity distributions in macroscopic objects does not contain the diffractive component that causes the suppression. Second, the maximum electric field occurs at the apex of the V-shape that confirms the observations of Suzuki *et al* [16].

A comparison of the energy flux:  $x$  and  $z$  components

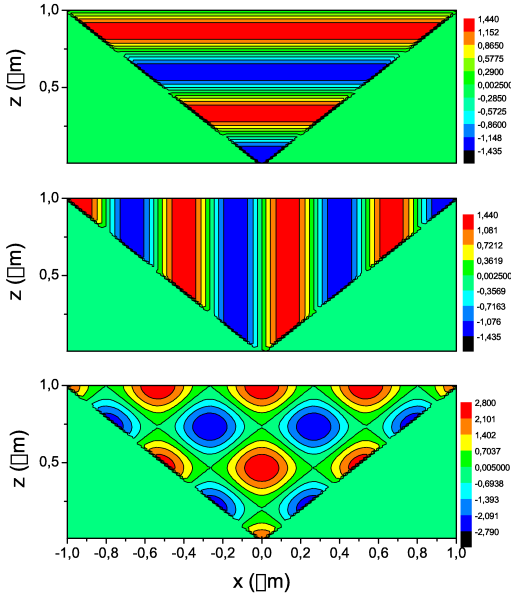


Figure 4:  $E_x$  and  $E_z$  electric and  $H_y$  magnetic field distributions (far-field theory)  $\lambda = 534$  nm.

of the Poynting vector are depicted in Figure 5. It is important to note that, while the standing waves appear at distances that satisfy the  $n\lambda/2$  criterium for the consecutive wavelengths, the values of intensity maxima of the standing waves are strongly wavelength dependent. This dispersion effect might influence the efficiency of Raman-enhancement in these structures when using different laser wavelengths, and could be used for the experimental verification of the predictions of the calculations. Note that enhancement at different wavelengths is not the same for electric field components and Poynting vector components, e.g. Poynting vector shows notable enhancement for  $\lambda = 534$  nm in comparison with  $\lambda = 434$  nm or  $\lambda = 634$  nm while for the same wavelength the maximal value of the electric field vector is the smallest.

In summary, theoretical analysis of light diffraction in a sub-wavelength to near-wavelength V-groove in a perfect conductor screen was performed by using near-field approach. It was shown that the geometry acts as an optical resonator where the intensity enhancement is determined by the near-field effects, i.e. without plasmons. The field vectors form vortices around the intensity maxima, being mostly parallel to the walls of the groove, which determines the Raman modes of surface bound molecules enhanced in this configuration. The intensity enhancement is wavelength dependent, thus different laser wavelengths might lead to different Raman enhancement when using this geometry. Comparison of results obtained with near-field and far-field approaches reveals that the near-field

component is responsible for the observed dramatic intensity enhancement, and thus the Raman enhancement as well.

Acknowledgement AM acknowledges the Australian Research Council and the support of Monash University through the Monash Fellowship scheme. This study was supported in part by the Framework for European Cooperation in the field of Scientific and Technical Research (COST, Contract No. MP0601) and the Hungarian Research and Development Program (KPI, Contract No. GVOP 0066- 3.2.1.-2004-04-0166/3.0).

- 
- [1] F. J. García-Vidal and J. B. Pendry, Phys. Rev. Lett. 77, 1163 (1996).
  - [2] J. LePerchec, P. Quemerais, A. Barbara, and T. Lopez-Rios, Phys. Rev. Lett. 100, 066408 (pages 4) (2008).
  - [3] S. Coyle, M. C. Netti, J. J. Baumberg, M. A. Ghanem, P. R. Birkin, P. N. Bartlett, and D. M. Whittaker, Phys. Rev. Lett. 87, 176801 (2001).
  - [4] N. M. B. Perney, J. García de Abajo, J. J. Baumberg, M. D. B. Charlton, M. E. Zoorob, A. Tang, and M. C. Netti, Physical Review B 76, 035426 (2007).
  - [5] Klarite, D3 Technologies, Glasgow, UK, URL <http://www.d3technologies.co.uk/>.
  - [6] G. Klemens and Y. Fainman, Optics Express 14, 9864 (2006).
  - [7] E. Betzig, A. Harootunian, A. Lewis, and M. Isaacson, Appl. Opt. 25, 1890 (1986).
  - [8] S. V. Kukhlevsky, M. Mechler, L. Csapo, K. Janssens, and O. Samek, Phys. Rev. B 70, 195428 (2004).
  - [9] M. Mechler, O. Samek, and S. V. Kukhlevsky, Phys. Rev. Lett. 98, 163901 (2007).
  - [10] T. Ebbesen, H. Lezec, H. Ghaemi, T. Thio, and P. Wolff, Nature 391, 667 (1998).
  - [11] J. A. Porto, F. J. García-Vidal, and J. B. Pendry, Phys. Rev. Lett. 83, 2845 (1999).
  - [12] J. B. Pendry, Science 285, 1687 (1999).
  - [13] A. Krishnan, T. Thio, T. Kim, H. Lezec, T. Ebbesen, P. Wolff, J. Pendry, L. Martín-Moreno, and F. García-Vidal, Opt. Commun. 200, 1 (2001).
  - [14] F. Baida and D. van Labeke, Opt. Commun. 209, 17 (2002).
  - [15] H. F. Schouten, T. D. Visser, G. Gbur, D. Lenstra, and H. Blok, J. Opt. A: Pure Appl. Opt. 6, S277 (2004).
  - [16] K. Suzuki, F. Koyama, and K. Iga, Electron. Comm. Jpn. 85, 20 (2002).
  - [17] F. J. García de Abajo, R. Gómez-Medina, and J. J. Sáenz, Phys. Rev. E 72, 016608 (2005).
  - [18] F. J. García-Vidal, H. J. Lezec, T. W. Ebbesen, and L. Martín-Moreno, Phys. Rev. Lett. 90, 213901 (2003).
  - [19] Q. Cao and P. Lalanne, Phys. Rev. Lett. 88, 057403 (2002).
  - [20] F. Neerhoff and G. Mur, Appl. Sci. Res. 28, 73 (1973).
  - [21] I. V. Novikov and A. A. Maradudin, Phys. Rev. B 66, 035403 (2002).
  - [22] D. Gramotnev and D. F. P. Pile, Appl. Phys. Lett. 85, 6323 (2004).
  - [23] D. F. P. Pile and D. K. Gramotnev, Opt. Lett. 29, 1069 (2004).

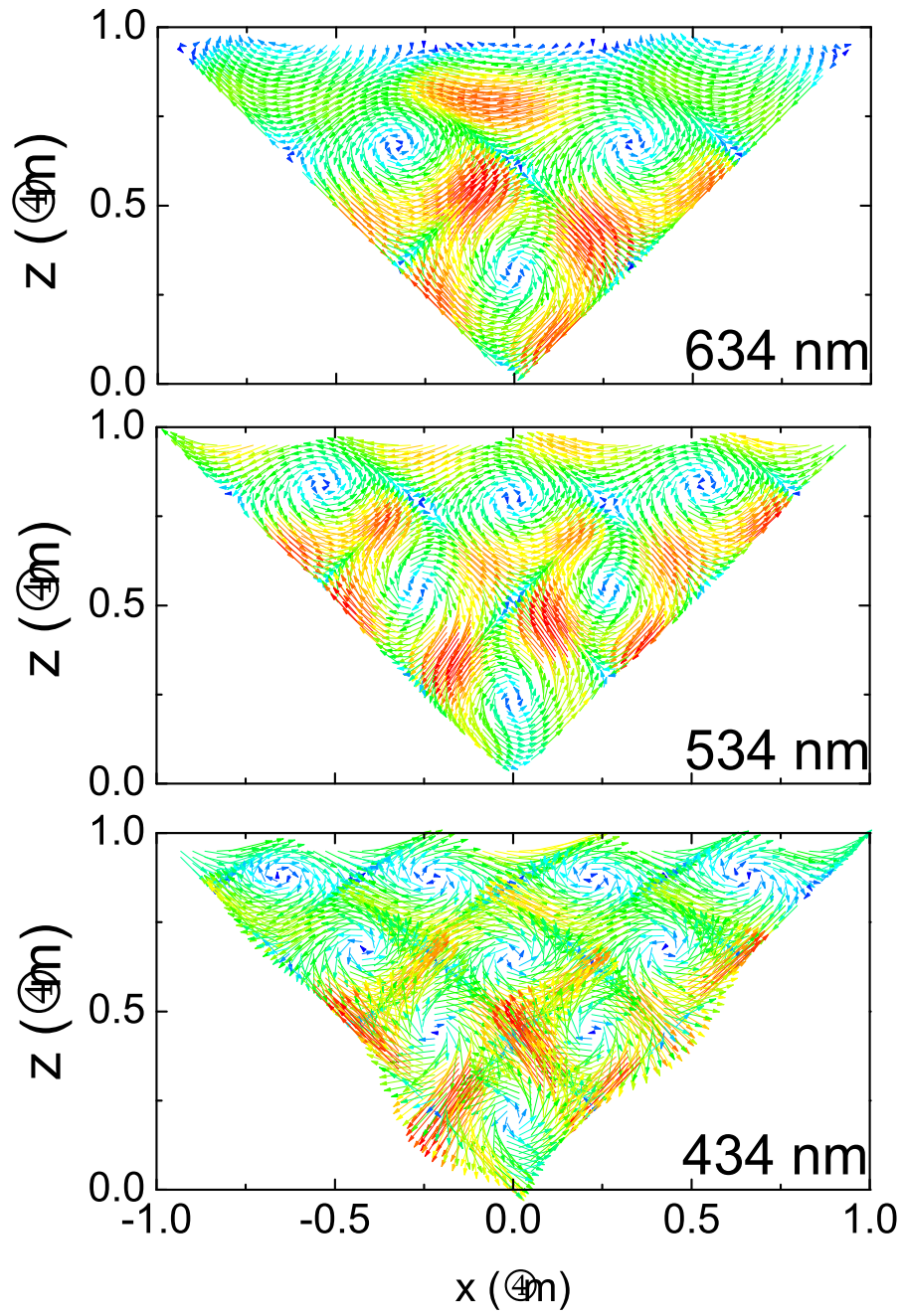


Figure 5: Poynting vector for three wavelengths: 434 nm, 534 nm and 634 nm. Note the “moving” of the standing wave.

- [24] D. F. P. Pile and D. K. Gramotnev, Appl. Phys. Lett. 86, 161101 (2005).
- [25] E. Moreno and S. G. Rodrigo and, S. I. Bozhevolnyi and, L. Martín-Moreno and, F. J. García-Vidal and, Phys.

- Rev. Lett. 100, 023901 (2008).
- [26] P. Morse and H. Feshbach, *Methods of Theoretical Physics* (McGraw-Hill, New York, 1953).